Research Article | Vol. 0, No. 0 / 00 00 0000 / Optics Express 1

Optics EXPRESS

Optimization and visualization of phase modulation with filtered and amplified maximal-length sequence for SBS suppression in a short fiber system: a theoretical treatment

YIFENG YANG,[1,2] BINGLIN LI,[1] MEIZHONG LIU,[1] XUCHEN HUANG,[2] YUTONG FENG,[2] DAN CHENG,[2] BING HE,[1,3] JUN ZHOU,[1] AND JOHAN NILSSON[2,4]

[1] *Shanghai Key Laboratory of All Solid-State Laser and Applied Techniques, Shanghai Institute of Optics and Fine Mechanics, Chinese Academy of Sciences, Shanghai 201800, China*
[2] *University of Southampton, Southampton SO17 1BJ, UK*
[3] *bryanho@siom.ac.cn*
[4] *jn@orc.soton.ac.uk*

Abstract: We use a model to investigate both the temporal and spectral characteristics of a signal lightwave which has been spectrally broadened through phase modulation with a maximal-length sequence (MLS), which is a common type of pseudo-random bit sequence. The enhancement of the stimulated Brillouin scattering (SBS) threshold of the modulated lightwave in a fiber system is evaluated by numerically simulating the coupled three-wave SBS interaction equations. We find that SBS can build up on a nanosecond-level time scale in a short fiber, which can reduce the SBS suppressing capability of MLS modulation waveforms with GHz-level clock rate, if the sub-sequence ("run") lengths with the same symbol (zero or one) of the MLS extend over several nanoseconds. To ensure the SBS buildup is perturbed and thus suppressed also during these long sub-sequences, we introduce a low-pass filter to average the signal over several bits so that the modulation waveform changes gradually even during long runs and amplify the RF modulation waveforms to the level required for sufficient spectral broadening and carrier suppression of the optical signal. We find that the SBS suppression depends non-monotonically on the parameters of the filtered and amplified MLS waveform such as pattern length, modulation depth, and the ratio of low-pass filter cutoff frequency to clock rate for maximum SBS mitigation. We optimize the SBS suppression through numerical simulations and discuss it in terms of the temporal and spectral characteristics of the lightwave and modulation waveform using derived analytical expressions and numerical simulations. The simulations indicate that the normalized SBS threshold reaches a maximum for a RMS modulation depth of 0.56π and a ratio of filter cutoff frequency to clock rate of 0.54 and that MLS9 is superior to other investigated patterns.

1. Introduction

Yb-doped fiber amplifiers (YDFAs) at wavelengths around 1 μm are well-established as reliable laser sources for high power and brightness [1,2]. Still, they are limited by nonlinearities, optical damage, and thermal problems [3–6]. Several beam combining schemes aiming to overcome their limitations were demonstrated in recent years [7–9]. Both spectral and coherent beam combining benefit from monolithic fiber amplifiers with narrow linewidth and good beam quality [10–13]. However, for those beam combining schemes, the nonlinear effect of stimulated Brillouin scattering (SBS) limits power scaling, and suppression techniques are therefore applied [14–16]. SBS is a spectrally narrow process that involves scattering off an acoustic wave. External phase modulation of a single-frequency seed laser with a temporal pseudo-random bit sequence (PRBS)

#426070 https://doi.org/10.1364/OE.426070
Journal © 0000 Received 25 Mar 2021; revised 9 May 2021; accepted 9 May 2021; published 00 00 0000

Optics EXPRESS

realized in the radio-frequency (RF) domain has been shown to be effective for broadening the spectrum and thus suppressing SBS [17,18]. The PRBS is normally a maximal-length sequence (MLS) of symbols (bits) "0" and "1". Control of the clock rate (i.e., the inverse of the bit duration) and pattern length of the MLS provides useful flexibility and control of the frequency spacing as well as of the total linewidth of the optical spectrum with the basic binary phase modulation between 0 rad (zero-symbol) and π rad (one-symbol), or more generally, between the zero-symbol phase ϕ_0 and $\phi_0 + \pi$. In this scenario, the optical phase can be varied faster than the SBS buildup time, which prevents the acoustic wave from building up to a large amplitude, and the SBS gain will be reduced consequently [19,20]. In addition, the effect of low-pass filtering and amplification of the MLS on the SBS suppression has been investigated [21,22]. However, despite the success and widespread use of MLS phase modulation for SBS suppression, reports of rigorous analytical expressions for the resulting optical spectra phase modulated with a MLS waveform and investigations of the temporal and frequency characteristics of MLS phase modulation are sparse [23]. Furthermore, the optimization of the waveform parameters, i.e., pattern length, clock rate, modulation depth, and filter bandwidth, for best SBS mitigation has yet to be reported in detail.

In this work, we report theoretical investigations of SBS suppression in a short passive fiber through MLS phase modulation of a single-frequency optical signal. Resulting optical spectra are found analytically by considering the MLS as a cyclostationary sequence. The dependence of the carrier and sideband components on the modulation depth (i.e., amplitude of the phase modulation) and the pattern length is illustrated. We introduce the triply coupled set of nonlinear partial differential equations to describe the SBS dynamics of the modulated optical signal, and solve it with numerical integration. It is shown that when unperturbed, the SBS can build up with a nanosecond-level time constant in a short fiber, which is faster than the decay constant of the acoustic wave. The buildup is quasi-exponential, and can therefore compromise the SBS suppressing capabilities of the MLS phase modulation, insofar as this has long uninterrupted sub-sequences (known as “runs") of the same symbol, which can extend over several nanoseconds. We introduce a low-pass filter to ensure the modulation waveform changes even during long runs, and use a RF amplifier to reach desired phase modulation depth. The dependence of the normalized SBS threshold and the RMS linewidth on the filter cutoff frequency and the phase modulation depth for MLS with different pattern lengths is investigated, and the optical spectra for some local maxima are illustrated. Aiming to accomplish the best SBS mitigation, parameters of the filtered and amplified MLS such as pattern length, modulation depth, and the ratio of filter cutoff frequency to clock rate are optimized numerically.

This paper is structured as follows. Section 2 describes the numerical model and the SBS dynamics. The SBS threshold and the buildup time for a short fiber system are investigated. In section 3, the temporal characteristics of the MLS waveform and the frequency characteristics of the phase modulated optical signal are discussed. Section 4 illustrate the SBS suppressing capability for unfiltered MLS phase modulation cases. Optimization of the filtered and amplified MLS phase modulation is investigated in Section 5. Section 6 concludes the paper.

2. Numerical model

The MLS phase modulation and SBS suppression scheme we consider is shown in Fig. 1. A single-frequency seed laser at 1075 nm (typically with linewidth less than 5 MHz) is externally modulated by an electro-optic phase modulator (EOPM). A MLS waveform in the RF domain is filtered by a low-pass filter and amplified by a RF amplifier and then drives the EOPM. The modulated lightwave is then amplified in an optical amplifier, the output of which is spliced to a passive delivery fiber with length L. The optical amplifier is assumed to be ideal, so does not introduce any distortions. Thus, the pattern length and the clock rate of the MLS, the RF power (related to the modulation voltage and depth), and the cutoff frequency of the filter control the

Optics EXPRESS

modulation and thus spectral broadening of the lightwave. We then consider the SBS dynamic in this passive fiber. Although SBS could also occur in the amplifier, this is not considered.

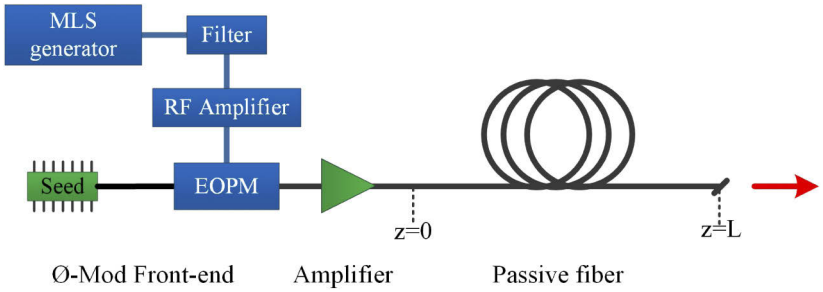

Fig. 1. Schematic diagram of the MLS phase modulation and short fiber system. $z = 0$ and $z = L$ denote the input and output end of the passive fiber. EOPM, electro-optic phase modulator.

The optical waves propagating in the fiber core can be represented by the electric field A_L of the forward propagating laser and the electric field A_S of the backward propagating Brillouin Stokes wave [17]. We do not consider the SBS seeding effect [21] that can occur when the linewidth exceeds the Brillouin frequency shift (~16 GHz for 1064 nm), because the spectral broadening in this work is small compared to that, and because it is possible to fine-tune the clock rate so that the spectral lines of the signal avoid the Brillouin gain peak [24]. Using the slowly varying envelope approximation and ignoring the group velocity dispersion and the background propagation losses (negligible in a short fiber), the temporal and spatial evolution of the laser, Stokes and acoustic fields in a fiber are determined by the following coupled system (corresponding to a Lorentzian Brillouin line):

$$\frac{c}{n}\frac{\partial A_L}{\partial z} + \frac{\partial A_L}{\partial t} = i\sigma\rho A_S \tag{1}$$

$$-\frac{c}{n}\frac{\partial A_S}{\partial z} + \frac{\partial A_S}{\partial t} = i\sigma\rho^* A_L \tag{2}$$

$$(\alpha - i)\frac{\partial \rho}{\partial t} - i\frac{\Gamma_B}{2}\rho = \chi A_L A_S^* - if \tag{3}$$

Here $\sigma = \omega\gamma_e/2n^2\rho_0$, $\chi = \epsilon_0\gamma_e k_q^2/2\Omega_B$, $\alpha = \Gamma_B/\Omega_B$, respectively. The phonon decay rate $\Gamma_B = 2\pi/17.5\ ns^{-1}$ [17] $= 2\pi \times 57.1 \times 10^6\ s^{-1}$. This is also the full-width at half-maximum (FWHM) of the Brillouin line in angular frequency. Thus, in "regular" frequency, the FWHM Brillouin linewidth $\Delta\nu_B$ becomes 57.1 MHz. The phonon lifetime τ_p is the inverse of the decay rate and becomes 2.79 ns. Furthermore, $\omega = 2\pi c/\lambda$ and $\Omega_B = 2n\nu_A\omega/c$ is the laser and resonant acoustic angular frequency, respectively. The acoustic wave number $k_q = 4\pi/\lambda$. The definition of some other parameters are like this: γ_e is the electrostrictive constant, ρ_0 is the mean density of the fiber medium, n is the core refractive index, c is the velocity of light in vacuum, ϵ_0 is the dielectric constant, ν_A is the speed of the acoustic wave, and ρ is the amplitudes of the acoustic wave, respectively. Since the second derivative of the acoustic field has negligible influence on the simulation results with low optical linewidths, we omit this term for simplicity. The quantity $f_{j,k} = \sqrt{ncQ/(\Delta t)^2}S_{j,k}$ in RHS of Eq. (3) represents the initiation of the SBS process from Langevinian noise [25], where $Q = 2k_B T_c \Gamma_B \rho_0/A\nu^2$, k_B is Boltzmann's constant, T_c is the temperature in the fiber core, and A is the fiber effective mode area, respectively. The quantity $S_{j,k}$ denotes a complex random function with Gaussian distribution of zero mean and unit variance. The indices j and k enumerate the spatial and temporal points of the numerical grid along the fiber and in time. The symbols Δz and Δt denote the spatial and temporal grid spacing,

Optics EXPRESS

respectively. The MLS coded phase modulation can be introduced by $A_L(0,t) = A_L(0,0)e^{i\phi(t)}$, where $\phi(t)$ is the optical phase coded by MLS waveform and $A_L(0,0)$ is the input laser amplitude at location $z = 0$. Given the noise seeding of SBS, the Stokes wave is often pulsing. The SBS level is therefore quantified by the time-averaged reflectivity $R = \langle|A_S(0,t)|^2\rangle/\langle|A_L(0,t)|^2\rangle$, where the brackets indicate time-averaging over several transit times (20 fiber transit times in this work). The SBS threshold is defined as the laser power that results in $R = 1\%$. The single-pass gain G, in units of nepers (Np), is defined by $G = g_pPL/A$, where P is the laser power at $z = 0$, and $g_p = \gamma_e^2\omega^2/\rho_0 nc^3 v_A\Gamma_B$ is the peak value of the Brillouin gain. The three-wave equations Eqs. (1)–(3) are solved numerically using the Euler method along the characteristic lines $dz/dt = \pm c/n$ [17]. We use the normalized SBS threshold to quantify the SBS suppression (or the SBS threshold enhancement factor). This is the ratio of the SBS threshold with phase modulation to the unmodulated SBS threshold. It is also equivalent to the multiplicative inverse for the normalized SBS gain introduced in Ref. [23], i.e., one is the inverse of the other. Parameters and the values we have used are shown in Table 1. The fiber length of 7.4 m leads to a single-pass transit time of 35.8 ns.

Table 1. Parameters and the values used for simulation 1mm

A	$2.6\times10^{-10}\ m^2$	n	1.45
T_c	$293.15\ K$	λ	$1075\ nm$
ω	$1.7534\times10^{15}\ rad/s$	ρ_0	$2201\ kg/m^3$
γ_e	1.95	v_A	$5.9\times10^3\ m/s$
L	$7.4\ m$	c	$3\times10^8\ m/s$
k_B	$1.38064852\times10^{-23}\ m^2Kgs^{-2}K^{-1}$	ϵ_0	$8.854187817\times10^{-12}\ F/m$
τ_p	$2.79\ ns$	$\Delta\nu_B$	$57.1\ MHz$

First of all, we use this numerical model to calculate the SBS threshold thus defined with no phase modulation. The dependence of the SBS reflectivity on the single-pass gain G is shown in Fig. 2(a). The fluctuation of the reflectivity is caused by the stochastic nature of the noise source and indicates the uncertainty resulting from the finite duration of the averaging. The threshold for 0.01 reflectivity is around $G = 9$ Np (~5 W) for the parameters above. We also examine the temporal evolution of the Stokes power at its output (at the signal input end of the passive fiber at $z = 0$) and investigate the details about the SBS buildup time at this location. The SBS buildup time can be defined as the delay between the start of the Stokes and that of the laser [26]. Here in our simulation, according to the relaxation oscillations in SBS dynamics, we evaluate the buildup process in terms of the time constant in the time before the reflectivity reaches its maximum value, during which the temporal evolution of the Stokes power shows an approximately exponential form. For this we introduce an ON-OFF-ON-like phase modulation with a MLS waveform with parameters such that SBS is well suppressed when the MLS is ON. The switch-OFF moment of the MLS waveform represents the starting point of the SBS buildup. The modulating scheme and the SBS reflectivity as a function of time for $G = 30$ Np and 150 Np are shown in Fig. 2(b), as calculated by ensemble averaging over 100 times of the SBS temporal evolution to reduce noise fluctuations. It shows a rapid growth of the Stokes power in the first several nanoseconds for large G (such as $G = 150$ Np), and then relaxation oscillations appear, which agrees with the statement in Ref. [27]. To further investigate the dependence of time constant on G, we also examine the SBS buildup kinetics in a modulation switch-OFF time period of 10 ns, which is shown in Fig. 2(c). The dashed curves show the exponential fitting curves. The time constants for different G calculated by the curve fitting are shown in Fig. 2(d). It is clear that the time constant is inversely proportional to G and in the nanosecond time scale. To be certain, SBS in a short fiber system can build up within several nanoseconds at high power, with a time constant that is considerably shorter than the transit time of the optical waves, and shorter than the phonon

Optics EXPRESS

lifetime. The smallest time constant becomes 0.9 ns in Fig. 2(d), which occurs for the highest considered single-pass gain of 200 Np, i.e., around 22 times the unbroadened threshold. Note that narrow-line fiber systems may well be broadened to a higher enhancement factor than this, e.g., 53 in [22], and we would then expect an even shorter time constant.

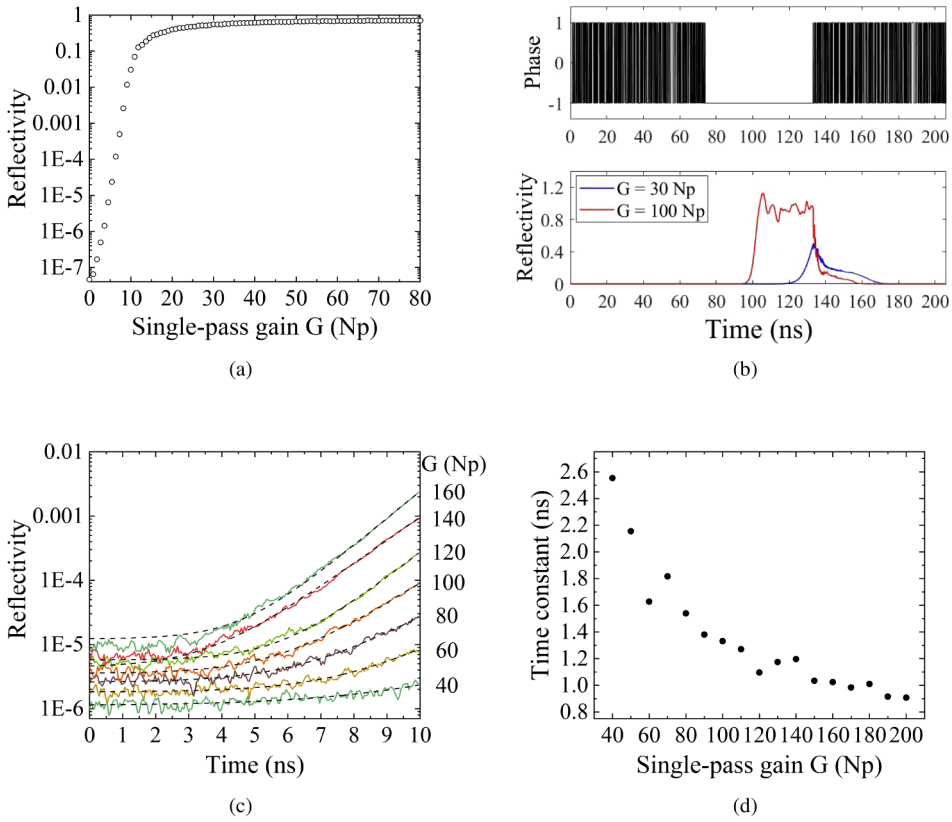

Fig. 2. (a) SBS reflectivity of unmodulated signal plotted as a function of the single-pass gain G (Np). (b) The ON-OFF-ON MLS phase modulation and the SBS dynamic for G = 30 Np and 150 Np. (c) The temporal evolution of SBS reflectivity for different single-pass gain G. (d) The time constant of the exponential growth of the Stokes wave as a function of G.

3. Temporal and frequency characteristics of MLS phase modulation

The maximal-length sequence is a type of PRBS which possesses all three PRBS randomness criteria simultaneously [28]. An MLS is sometimes called an m-sequence or n-sequence, and can also be denoted as PRBSn or MLSn. It is commonly used in spread spectrum systems, bit error testing, and many other areas, and can be easily produced by a Linear Feedback Shift Register (LFSR) of length n. Mathematically, the maximal-length sequences are described by irreducible and primitive polynomials [29]. For MLS3, the polynomial is $x^3 + x + 1$, or abbreviated as (3,1,0). Correspondingly, there are (5,2,0) for MLS5, (7,1,0) for MLS7, (9,4,0) for MLS9, (11,2,0) for MLS11, (13,4,3,1,0) for MLS13, and (17,3,0) for MLS17, respectively. A MLS consists of an aperiodic base sequence of length $N = 2^n - 1$, which is then periodically repeated to form a continuous infinite sequence, and since it is periodically repeated, its bit sequence (or pattern) has a discrete spectrum with frequency spacing equal to the inverse of the period.

Optics EXPRESS

The choice of the pattern length in MLS phase modulation in fiber system has always been a dilemma. If the pattern of the MLS is too short then the line spacing can become excessive and the number of spectral lines small, and the power per spectral line thus too high for efficient SBS suppression. On the other hand, the phase for a MLS phase modulated lightwave stays constant during the uninterrupted sub-sequences ("runs"), which could also lead to significant SBS in a fiber system if these sub-sequences are too long (large n). This suggests that there is a length that optimizes the trade-off between these conflicting considerations. In addition, with low-pass filtering, the MLS waveform is averaged over several bits due to significant inter-symbol interference (ISI) when the filter cutoff frequency is small compared to the clock rate. Thus, the phase can vary continuously, and SBS suppressed, even during long runs. Although averaging also reduces the amplitude of the modulation, this can be restored through amplification of the low-pass filtered RF wave. This control of the RF power (i.e., modulation amplitude) further extends the control of the optical spectrum. The temporal and frequency characteristics of unfiltered and filtered and amplified MLS phase modulation are important for the understanding of the SBS suppression capability.

In this Section, we investigate the temporal characteristics of the MLS waveform (Section 3.1), the optical spectra of MLS phase modulation (Section 3.2), and the optical spectra of filtered and amplified MLS phase modulation (Section 3.3).

3.1. Temporal characteristics of a MLS waveform

The properties of a MLS waveform are controlled by the sequence

$$\{a_j\} = \{a_0, a_1, \ldots, a_{N-1}\} \tag{4}$$

The quantity $\{a_j\}$ is a variable with a period of N that takes on discrete values -1 (if the bit is symbol 0) and +1 (if the bit is symbol 1). If an element from the sequence is chosen at random, then the probabilities of the different values become $Pr_{+1} = (1 + 1/N)/2$ and $Pr_{-1} = (1 - 1/N)/2$, respectively, where of course $Pr_{+1} + Pr_{-1} = 1$. To form a continuous waveform (e.g., for modulation) from the sequence, a single period $x_N(t)$ of the continuously repeated train $x(t)$ can be written as

$$x_N(t) = \sum_{j=0}^{N-1} a_j p(t - jT) = p(t) * \sum_{j=0}^{N-1} a_j \delta(t - iT) \tag{5}$$

where T is the bit duration (equal to the inverse of the clock rate f_{cr}) and $*$ denotes convolution. The base shape $p(t)$ of a single symbol is assumed to be the same for both types of symbols. It is often taken to be a rectangular function, constant throughout the duration T of the symbol slot and zero outside, and can thus be written as

$$p(t) = \begin{cases} 1 & 0 \le t \le T \\ 0 & otherwise \end{cases} \tag{6}$$

The intermediate aperiodic signal $x_N(t)$ can then be extended in time by using a comb of delta functions with a time spacing of $T_N = NT$. This operation can be formulated as convolution resulting in the periodic train

$$x(t) = p(t) * \sum_{j=0}^{N-1} a_j \delta(t - jT) * \sum_{k=-\infty}^{\infty} \delta(t - kT_N) \tag{7}$$

where $j, k \in \mathbb{Z}$ are used to specify discrete instants in time. For the purpose of comparing the characteristics of MLS with different base sequence lengths N, we plot normalized values in one

Optics EXPRESS

period T_N for sequences with N = 31, 127, 511, and 2047 bits (n = 5, 7, 9, 11) with a clock rate of 6.5 GHz, shown in Fig. 3(a). The signal filtered by a low-pass filter with a cutoff frequency of 2.2 GHz is shown in Fig. 3(b). We choose a low-pass filter with the amplitude characteristics of a 6^{th}-order Butterworth filter in this paper, because we have found that to agree well with the filtering in our previous experimental work [22]. However, the filter is of the zero-phase type, i.e., with flat phase characteristics. Such a filter is not causal but the resulting signal can still be generated by an arbitrary waveform generator (AWG) with pre-calculated sample values. We use Matlab's "filtfilt" function to implement zero-phase filtering [30]. It is clear in Fig. 3(b) and Fig. 3(d) that the normalized phase spreads beyond the range (-1, 1) and also attains intermediate values.

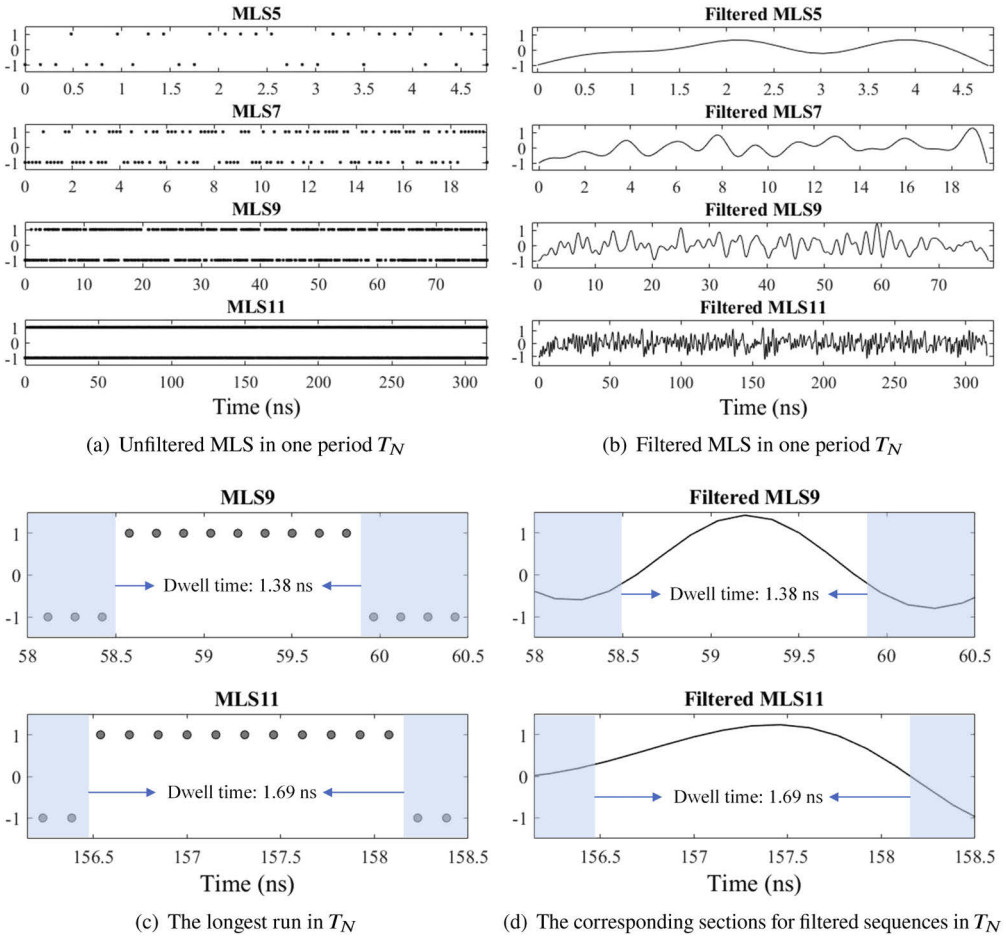

(a) Unfiltered MLS in one period T_N

(b) Filtered MLS in one period T_N

(c) The longest run in T_N

(d) The corresponding sections for filtered sequences in T_N

Fig. 3. Normalized MLS-based phase sequences according to Eq. (5) in one period for MLS5, MLS7, MLS9, and MLS11 with 6.5 GHz clock rate. (a) Unfiltered MLS, one dot represents one bit, that is T = 0.1538 ns in our case. (b) MLS filtered by zero-phase low-pass filter with the amplitude response of a 6^{th}-order Butterworth filter with a cutoff frequency of 2.2 GHz. (c) Enlargement over the longest run in a single period (T_N) of MLS9 and MLS11. (d) The corresponding sections for the longest runs in filtered MLS9 and MLS11.

We next consider the temporal properties of MLS and compare them to the SBS buildup time. A MLSn sequence contains 2^{n-1} runs, including one single "1" run of length n (the "dwell time" in Ref. [17]), which is the longest run, and 2^{n-1-i} runs of length i, where i = 1, 2, 3, . . ., n-1.

Optics EXPRESS

This includes the second-longest run, which comprises n-1 of “0". For shorter runs, there are the same number of zero-runs and one-runs. Take MLS9 for example, there are a total of 256 runs, which include a single run of ones of length 9, a single run of zeros of length 8, 2 runs of length 7, 4 runs of length 6, 8 runs of length 5, 16 runs of length 4, 32 runs of length 3, 64 runs of length 2, and 128 runs of length 1. We plot the longest run of MLS9 (1.38 ns) and MLS11 (1.69 ns) before (Fig. 3(c)) and after Fig. 3(d) filtering. The dwell time nT as a function of clock rate for n = 3, 5, 7, 9, 11, 13, 17, and 31 is shown in Fig. 4(a). For clock rates ranging from 3 GHz to 10 GHz, the dwell times for patterns considered in this work are within several nanoseconds, which are comparable to that of the SBS buildup time constant in the 7.4-m of passive fiber that we consider. Such dwell times may then lead to significant SBS, which will be demonstrated in Section 4. The amplitude of the low-pass filtered MLS waveform no longer stays constant (Fig. 4(b), which may then allow for better SBS suppression, although a small bandwidth may lead to excessive averaging. Also, the dependence of the period NT on clock rate for different MLS patterns is shown in Fig. 4(b). As seen, the period is much longer than the SBS buildup time (except for MLS3). In many cases, it is also longer than the 35.8 ns fiber transit time.

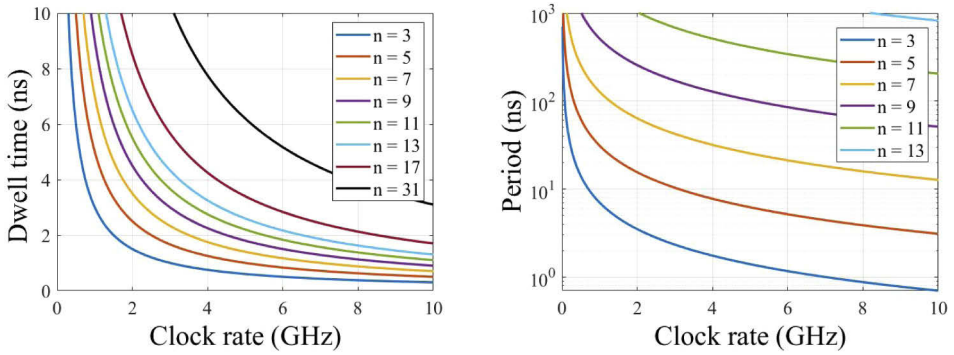

Fig. 4. (a) The length of the longest uninterrupted sub-sequence (or dwell time) nT vs. clock rate and (b) the period NT vs. clock rate for different patterns.

3.2. *Optical spectra of MLS phase modulation*

In this section, we discuss the optical spectra of lightwave phase-modulated with a MLS. We consider a linearly polarized single-frequency laser electric field

$$E(t) = \bar{E_L} Re\{e^{i[\omega_c t + \phi(t)]}\} \tag{8}$$

where $\bar{E_L}$ is the constant amplitude of the laser field, which we ignore in the calculation of the power spectral density for simplicity. For convenience, we shift the optical spectrum by the carrier frequency ω_c to be centered around $\omega = 0$. According to the expression given by Eq. (7), the MLS coded phase $\phi(t)$ can be represented as

$$\phi(t) = \frac{k_p}{2} p(t) * \sum_{j=0}^{N-1} a_j \delta(t - jT) * \sum_{k=-\infty}^{\infty} \delta(t - kT_N) \tag{9}$$

where k_p is the peak-to-peak phase modulation amplitude, which is defined as π times the ratio of the peak-to-peak modulation voltage to the half-wave voltage V_π of the EOPM. Here, the laser electric field $E(t)$ is an infinitely repeated periodic sequence with a period of N which takes two distinctive values $exp(ik_p/2)$ and $exp(-ik_p/2)$ (i.e., the phase $\phi(t)$ takes two values $k_p/2$ and

Optics EXPRESS

$-k_p/2$). Based on these properties, we can then calculate the autocorrelation function (ACF) of $E(t)$ as phase modulated by the MLS waveform. Recalling the periodic ACF (i.e., PACF) of a complex function (i.e. $E(t)$ in our case) at discrete times $\tau = kT$ is defined by

$$R_{x,x}(\tau) = \frac{1}{N}\sum_{j=0}^{N-1} x_j x_{j+\tau} \tag{10}$$

where $x_j x_{j+\tau}$ is the product of one bit in the base sequence with a corresponding bit shifted by kT, where j and k are integers. Figure 5 illustrates the evaluation of the PACF $R_{E,E}$ of $E(t)$ phase modulated by MLS3 for $k = 0, 1$, and 2, according to Eq. (10). The calculating procedure is shown in Fig. 5. The first period of $R_{E,E}$ can be expressed as

$$R_{E,E}(t) = \begin{cases} 1 - (1 + \frac{1}{N})sin^2(\frac{k_p}{2})\frac{|t|}{T} & 0 \le \frac{|t|}{T} \le 1 \\ cos^2(\frac{k_p}{2}) - \frac{1}{N}sin^2(\frac{k_p}{2}) & 1 \le \frac{|t|}{T} \le \frac{N}{2} \end{cases} \tag{11}$$

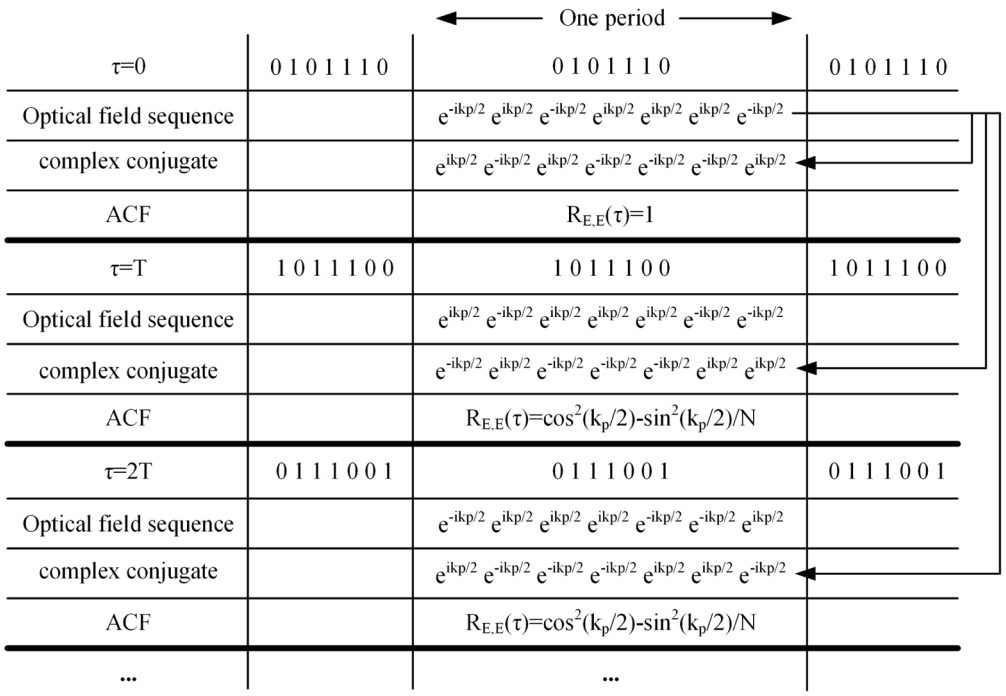

Fig. 5. An example calculation of the ACF for MLS3 phase modulated optical field.

The minimum value of $R_{E,E}$ varies in the range of $(-1/N, 1)$ according to k_p, which is shown in Fig. 6. The power spectral density (PSD) of the laser field can then be given by the Fourier transform of the PACF according to the Wiener-Khinchin theorem, that is

$$\begin{aligned} S_{E,E}(f) = \mathscr{F}\{R_{E,E}(\tau)\} = \mathscr{F}\left\{R_{E,E}(\tau) - cos^2\left(\frac{k_p}{2}\right) + \frac{1}{N}sin^2\left(\frac{k_p}{2}\right)\right\} \\ - \mathscr{F}\left\{cos^2\left(\frac{k_p}{2}\right) - \frac{1}{N}sin^2\left(\frac{k_p}{2}\right)\right\} \end{aligned} \tag{12}$$

Optics EXPRESS

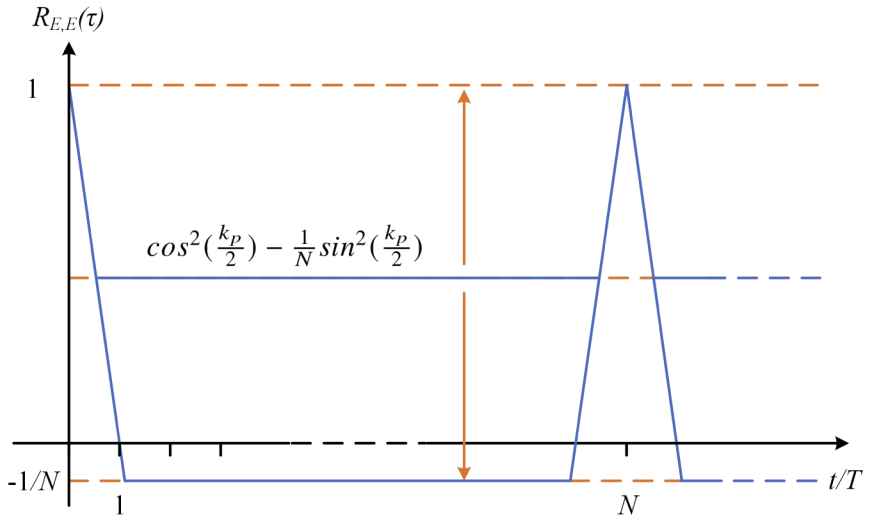

Fig. 6. PACF of the MLS phase modulated optical field, normalized by $\bar{E_L}$.

Through the use of elementary Fourier transform pairs and arithmetic, we can substitute Eq. (11) into Eq. (12), whereby Eq. (12) becomes

$$S_{E,E}(f) = \left[\frac{1+cos(k_p)}{2} + \frac{1}{N^2}\frac{1-cos(k_p)}{2}\right]\delta(f) + \frac{1-cos(k_p)}{2}\frac{N+1}{N^2} \times sinc^2\left(\frac{f}{f_{cr}}\right)\sum_{\substack{i=-\infty \\ i\neq 0}}^{\infty}\delta(f - if_N) \tag{13}$$

Equation (13) is the normalized optical spectrum of the MLS phase modulation scheme, which is a discrete spectrum. The line spacing is given by $f_N = 1/NT = f_{cr}/N$ and the clock rate f_{cr} and the modulation amplitude k_p determine the bandwidth. With a clock rate of 6.5 GHz, the line spacing becomes 928.57 MHz, 209.68 MHz, 51.18 MHz, 12.72 MHz, and 3.18 MHz for $n = 3, 5, 7, 9$, and 11, respectively. Spectral nulls occur at integer multiples of clock rate. The first part in RHS of Eq. (13) corresponds to the intensity (i.e., optical power) of the carrier while the second part corresponds to the intensity of the sidebands. The dependence of the intensities of the carrier and the adjacent sideband components on k_p is shown in Fig. 7(a) and 7(b). When $k_p = (2m+1)\pi$ ($m \in \mathbb{Z}$), Eq. (13) becomes the PSD of the MLS waveform [28], viz

$$S_{E,E}(f) = \frac{1}{N^2}\delta(f) + \frac{N+1}{N^2}sinc^2\left(\frac{f}{f_{cr}}\right)\sum_{\substack{i=-\infty \\ i\neq 0}}^{\infty}\delta(f - if_N) \tag{14}$$

At this point, the carrier reaches its lowest intensity $1/N^2$ and the adjacent sideband components reach their highest intensity $(N+1)/N^2$. If there is dominating spectral line with more power than in other lines then it is well known that the SBS threshold is dictated mainly by this line, when the optical sidebands act independently (approximately when $f_N > \Gamma_B/\pi$) [17]. It is clear from Fig. 7(a) and 7(b) that the carrier can be such a dominant component. Most importantly, this must not be excessive, but nor should it be depleted of power since this would mean that the other lines carry more power than necessary. Thus, a value of k_p that leads to the same carrier component intensity as in the adjacent (or the strongest) sideband components may be best for SBS suppression at large line spacing. The strengths of carrier and the adjacent sideband

Optics EXPRESS

components are compared in Fig. 7(c). We find that the values of k_p that lead to the same intensity in the carrier and the adjacent sideband components ($I_c = I_s$) are 0.8869π for MLS5, 0.9437π for MLS7, 0.9719π for MLS9, and 0.9859π for MLS11, respectively, as shown in Fig. 7(d). There are also equivalent points for k_p slightly larger than π. However, the power in the strongest spectral line varies only slowly near $k_p = \pi$ for every n (see Fig. 7(c)). Therefore, we take $k_p = \pi$ for the SBS suppression optimization for unfiltered MLS phase modulation in this work. Although this leads to marginally higher power in the strongest lines than necessary, this does not necessarily translate to a lower SBS threshold for small line spacings. Furthermore, we note that for most values of k_p, the carrier is the dominant line and needs to be controlled precisely if it is to match the highest sideband peak. The slow variation of the power in the carrier around $k_p = \pi$ reduces the sensitivity to errors in k_p.

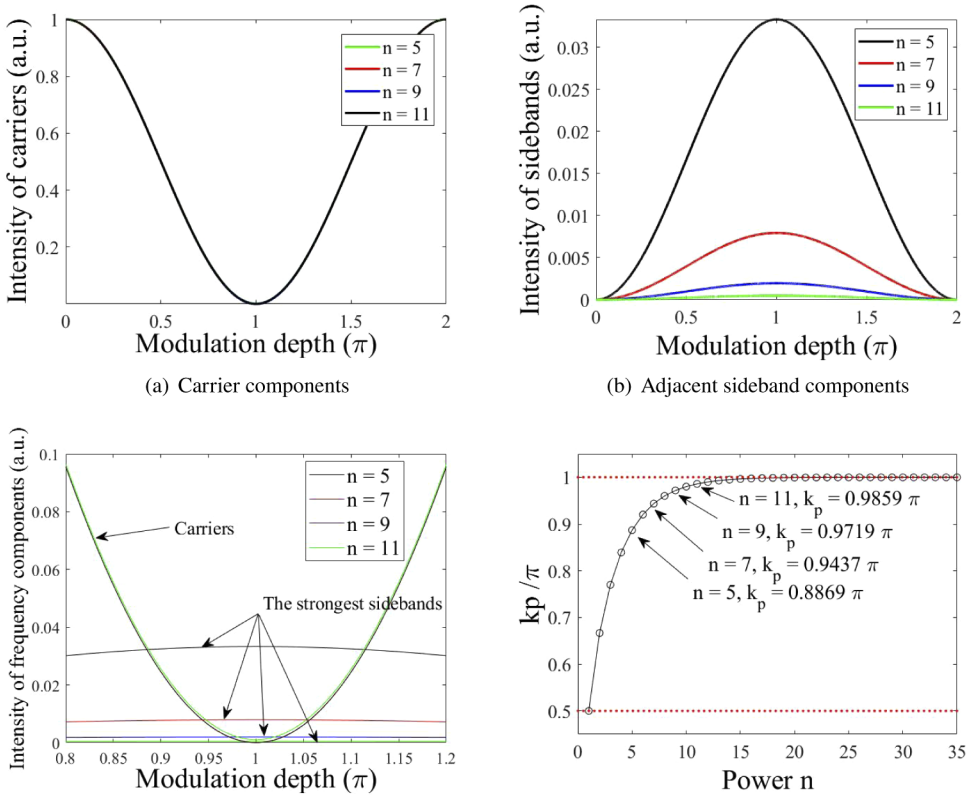

(a) Carrier components

(b) Adjacent sideband components

(c) Comparison of carriers and the adjacent sidebands

(d) k_p vs. n for $I_c = I_s$

Fig. 7. Intensity of (a) the carrier and (b) the adjacent sideband components vs. k_p for $n = 5, 7, 9$, and 11. (c) Intensity of the carrier and the strongest sideband components around $k_p = \pi$ for different n. (d) Values of k_p that lead to the same intensity in the carrier and the adjacent components for different power n.

To verify the derivation, we construct a series of MLS waveforms with $n = 5, 7, 9, 11$, and calculate numerically the PSD of the MLS phase modulated laser field using the Wiener-Khinchin theorem. The clock rate is 6.5 GHz, and the modulation depth assumes the values π, 1.12π, 1.3π, and 2π. The calculated results are shown in Fig. 8. The intensity of both carrier and sidebands are in good agreement with the derivation. The results confirm that when $k_p = \pi$, the carrier nearly vanishes and the sidebands reach their highest intensity. From these results we expect that

Optics EXPRESS

in this scheme, errors in k_p can easily result in a large carrier and thus drastically degraded SBS threshold.

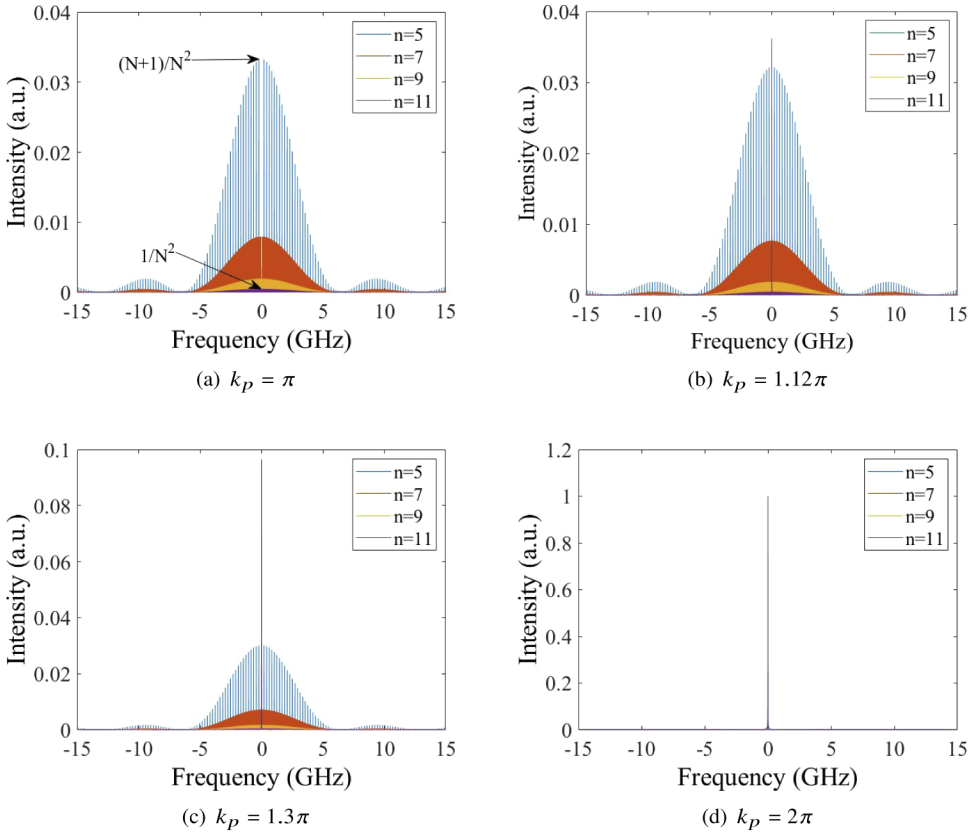

Fig. 8. Optical spectra for MLS phase modulation with $n = 5, 7, 9, 11$, and $f_{cr} = 6.5$ GHz for k_p equal to (a) π, (b) 1.12π, (c) 1.3π, and (d) 2π. Note the different vertical scales in (c) and (d).

3.3. *Optical spectra of filtered and amplified MLS phase modulation*

So far, the spectra of the phase modulated optical field are easy to find analytically because the unfiltered MLS is a sum of rectangular pulses. However, the spectra are sinc-shaped with slow decaying sidelobes, which is often undesirable, as is the distinctive behavior of the carrier. On the other hand, the bandwidth of rectangular pulses is infinite, so they will be distorted by the limited bandwidth of the different parts of a real system, in particular if there is a filter. As before, we will assume that a low-pass filter akin to a 6^{th}-order Butterworth filter but with spectrally flat phase characteristics determines the overall response. All other components are ideal, with bandwidth significantly larger than that of the filter, but other linear filter would be straightforward to implement. With reference to Fig. 1, the complex envelope at the RF input of the EOPM may be written as $\phi(t) * h(t)$, where $h(t)$ is the impulse response of the filter. The frequency-domain response for a Butterworth low-pass filter is $1/\sqrt{1 + (f/f_{co})^{2m}}$, where f_{co} is the cutoff frequency (-3dB) and m is the order. The electric field of the lightwave phase modulated by this filtered signal can be described as

$$E'(t) = \bar{E}_L Re\{e^{i[\phi(t)*h(t)]}\} \tag{15}$$

Optics EXPRESS

We have not been able to obtain an analytical expression for the spectrum of a lightwave phase modulated according to Eq. (15). Instead, we calculated spectra numerically. The modulation depth of the low-pass filtered and amplified MLS is defined as $k_\sigma = \pi V_\sigma / V_\pi$, where V_σ is the standard deviation of the voltage of the modulation waveform. This is related to the RMS voltage according to $k_\sigma = \sqrt{k_{RMS}^2 - k_{AVG}^2}$, where k_{AVG} is the average of the modulation depth. Thus, the RMS value and the standard deviation are equal if $k_{AVG} = 0$. We note that for an unfiltered MLS phase modulation with a peak-to-peak modulation amplitude of k_p, the modulation depth $k_{RMS} = k_p/2$ when MLS waveform takes the values of $-\pi/2$ or $\pi/2$. Although $k_{AVG} \neq 0$, the resulting difference is small, especially for a long MLS, and therefore we neglect it. Optical spectra for $n = 3, 5, 7, 9, 11$, and 13 with $f_{cr} = 6.5$ GHz are calculated with the ratio of the low-pass filter cutoff frequency to clock rate $f_{co}/f_{cr} = 0.4$, and $k_\sigma = 0.5\pi, \pi, 1.2\pi, 1.5\pi$, and are shown in Fig. 9. The spectra become wider as k_σ increases, and whereas the temporal periodicity means the spectra remain discrete, the envelopes are no longer $sinc^2$ shaped. There are no clear sidelobes, and, significantly, the power in the carrier does not depend critically on the modulation depth, at least for $k_\sigma > \pi/2$. Still, the carrier is in many cases the strongest component by a considerable margin, which may lead to SBS. Next, we will investigate the SBS suppression capability of unfiltered and filtered MLS phase modulation scheme numerically, including the impact of the spectral spikes. We start with the unfiltered case in the next section.

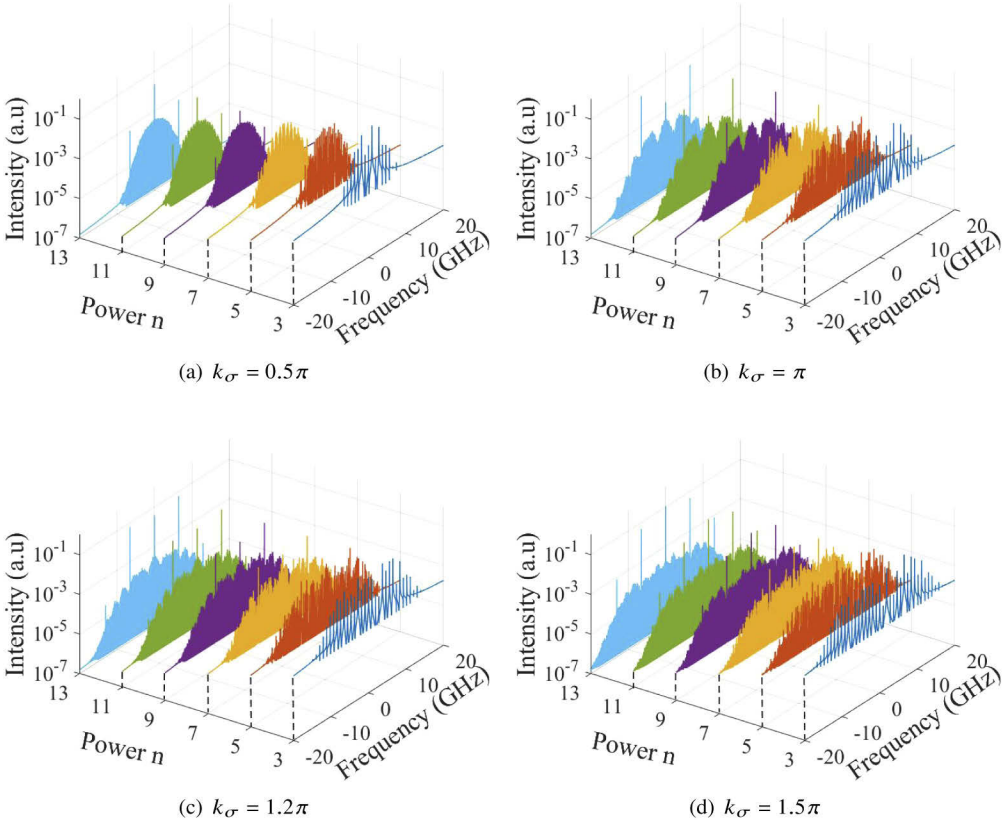

(a) $k_\sigma = 0.5\pi$ (b) $k_\sigma = \pi$

(c) $k_\sigma = 1.2\pi$ (d) $k_\sigma = 1.5\pi$

Fig. 9. Optical spectra as phase modulated by filtered and amplified MLS waveform with $f_{cr} = 6.5$ GHz, $f_{co}/f_{cr} = 0.4$, and $n = 3, 5, 7, 9, 11$, and 13 for k_σ equal to (a) 0.5π, (b) π, (c) 1.2π, and (d) 1.5π.

Optics EXPRESS

4. SBS suppression with unfiltered MLS phase modulation

As mentioned previously, phase modulation by an unfiltered MLS can provide an effective way of suppressing the SBS gain. We examine SBS suppression with phase modulation by a MLS with $k_p = \pi$ (approximate to $k_\sigma = \pi/2$) using the simulation method introduced in Section 2. This modulation amplitude avoids strong spectral lines in the optical spectrum (see Fig. 8). The normalized SBS threshold (i.e., the enhancement factor) as a function of clock rate for different bit patterns is shown in Fig. 10(a). It should be noted that, even though the normalized SBS threshold is calculated by time averaging over 20 transit times, there is still some residual randomness in the simulation results, due to the Langevinian noise introduced in every temporal and spatial grid point. The increase in enhancement factor with clock rate saturates for MLS3 and MLS5, for a clock rate of ~1.7 GHz (line spacing ~243 MHz) and ~7.5 GHz (line spacing ~242 MHz), respectively. Also, a rollover point of about 30 GHz can be obtained for MLS7 (line spacing ~236 MHz), which is shown in Fig. 10(b). The spectral line separation is more than twice the spontaneous Brillouin linewidth $\Delta\nu_B$ of 57.1 MHz in this paper at these points. For clock rates higher than these points, the spectral lines act independently and the SBS threshold no longer grows [17]. For high SBS threshold, the power should then be distributed over a large number of spectral lines, without excessive power in any line. Thus, in that regime, spectral considerations suggest a long MLS with smaller line spacing is preferable. However, once the spectral line spacing becomes sufficiently small for cross-interactions (beating) between adjacent spectral lines to contribute to the SBS gain, the SBS threshold decreases.

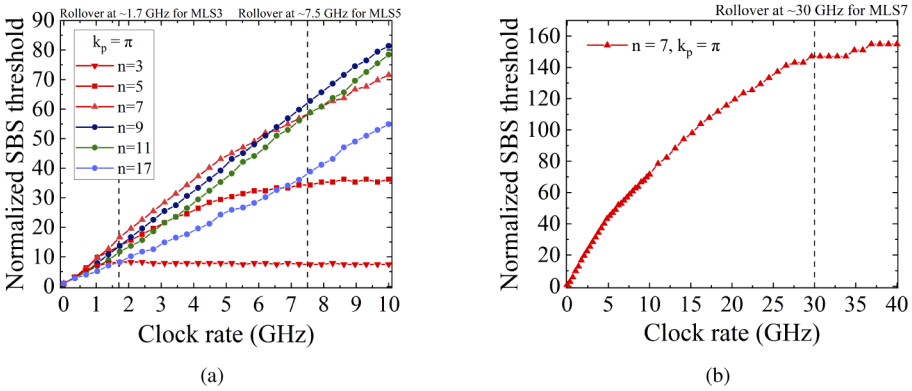

Fig. 10. Normalized SBS threshold with unfiltered MLS and $k_p = \pi$ vs. clock rate for (a) n = 3, 5, 7, 9, 11, and 17 for clock rates from 0 GHz to 10 GHz, and (b) n = 7 for clock rates from 0 GHz to 30 GHz.

It is shown in Fig. 10(a) that the SBS threshold enhancement with MLS11 is smaller than with MLS9 and that with MLS17 is smaller than with MLS9 as well as with MLS11. Thus, the shorter sequences are better, and we note that all of these sequences have line spacings smaller than the Brillouin linewidth for the range of clock rates plotted in Fig. 10(a). The largest spacing becomes 10 GHz / 511 = 19.6 MHz. This is often explained as a result of the smaller line spacing of the longer sequences (= f_{cr}/N), but in the simulations in [16], smaller line spacing, down to 12.5 MHz (the smallest considered) led to better SBS suppression for optimized, non-MLS, waveforms. However, this is not always the case, and a temporal-domain description may provide more insight into why one waveform should be better than the other, than the line spacing does. This includes MLS sequences, for the situation that the clock rate is sufficiently low relative to the rollover point. Then we believe that the dwell time for the MLS signal plays an increasingly important role in the SBS buildup kinetics, and for the same clock rate, the dwell time for MLS11 is longer than MLS9 (shown in Fig. 4(a)). For example, the dwell time for MLS9 and MLS11

Optics EXPRESS

with a clock rate of 1.5 GHz is 5.99 ns and 7.33 ns, respectively. Given that the Stokes power grows exponentially when the signal is unmodulated (Fig. 2(c)), for the case of G = 160 Np (corresponding to an enhancement factor of ~18 relative to the unbroadened threshold gain of 9 Np), the reflectivity can grow up to 6.13×10^{-5} for 5.99 ns and 1.91×10^{-4} for 7.33 ns, which means the reflectivity of the MLS11 case is 3 times than that of the MLS9 case. It is clear that there can be a significant penalty for the longer dwell time of MLS11. For MLS17, the dwell time is much longer still, and its SBS suppressing capability thus reduced.

5. Optimization of filtered and amplified MLS phase modulation

In this section, we numerically optimize a filtered and amplified MLS waveform used to drive a phase modulator for the best SBS mitigation. Still, we use a low-pass filter similar to a 6^{th}-order Butterworth filter but with zero phase. As a starting point, we investigate the SBS suppression capability for phase modulation with low-pass-filtered MLS (no RF amplification). A plot of the normalized SBS threshold vs. clock rate for different f_{co}/f_{cr} and $k_p = \pi$ for MLS9 is shown in Fig. 11(a). It is shown that the SBS threshold increases with f_{co}/f_{cr} for $k_p = \pi$. The highest threshold is reached for the unfiltered case (with infinite f_{co}). The reason for this is that the low-pass filtering is equivalent to temporal averaging, whereby the modulation depth k_σ becomes too small, leaving too much power in the carrier for effective SBS suppression (shown in Fig. 9).

To overcome this and achieve a high SBS threshold also with the low-pass filter, we use a RF amplifier to boost the modulation depth of the filtered MLS9 waveform. Then we investigate the dependence of normalized SBS threshold on the clock rate at $f_{co}/f_{cr} = 0.4$ for different modulation depth k_σ, which is shown in Fig. 11(b). As EOPMs often have a maximum RF input power of around 28 dBm into 50 Ω impedance (thus RMS voltage of 5.6 V) and a half-wave voltage around 5 V, the modulation depth K_σ in our calculations is chosen to be within π (corresponding to 27 dB). We note that the unfiltered case with $k_p = \pi$ (thus with $k_\sigma = \pi/2$) approximately matches the filtered case with $k_\sigma = \pi$. We plotted k_σ/k_p as a function of f_{co}/f_{cr} for different n, as shown in Fig. 11(c). For large values of filter cutoff frequency, k_σ is close to $k_p/2$.

Although Fig. 11 suggests that higher cutoff frequency and modulation are better, this is not generally the case. Figure 12(a) shows the dependence of the normalized SBS threshold on both f_{co}/f_{cr} and k_σ. The value of f_{cr} is chosen to be 10 GHz, which is a typical value. We note that within the parameter range investigated in Fig. 12(a), f_{co}/f_{cr} must be at least around 0.1. Furthermore, for large f_{co}/f_{cr}, good suppression is only achieved when k_σ equals an integer multiple of $\pi/2$. From a design perspective for filtered and amplified MLS phase modulation with a high SBS suppression, the optical linewidth plays an important role in this optimization. Figure 12(b) shows corresponding contours of the RMS linewidth $\Delta\nu_{RMS}$ according to these two parameters. Often, a narrow linewidth is preferred, and it is then desirable to suppress SBS with the smallest possible linewidth broadening. It is often assumed that the SBS threshold increases linearly with linewidth, and, the ratio of the normalized SBS threshold to $\Delta\nu_{RMS}$ is used as a figure of merit. This ratio is plotted in Fig. 12(c). Generally, there is significant structure with large variations in the plot, and the local maxima for normalized SBS threshold follows approximately a $k_\sigma = [0.06/(f_{co}/f_{cr} - 0.1) + 0.5] \times \pi$ behavior, where $f_{co}/f_{cr}>0.1$. We especially consider five local maxima in Fig. 12(c) (marked in red circles), and calculate the optical spectra using parameters in these zones, as shown in Fig. 13. It is interesting to note that there are no strong side bands in Fig. 13(a) and Fig. 13(b) (local maximum 1 and 2, respectively), whereas the other three local maxima (Fig. 13(c)–Fig. 13(e)) exhibit spectral "spikes" located at integer multiple of f_{cr}. In addition, the carriers are suppressed in all these five local maxima. It may safe to draw the conclusion that the suppression of the carrier and the strong sidebands for the filtered and amplified MLS phase modulation is necessary for SBS threshold enhancement in a fiber system.

Optics EXPRESS

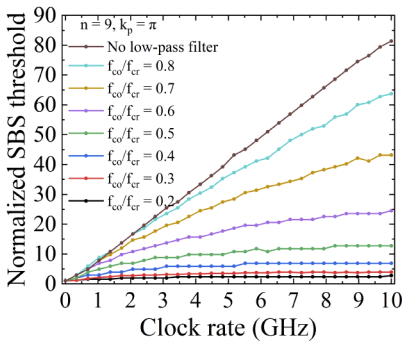

(a) with low-pass filter for different values of f_{co}/f_{cr}

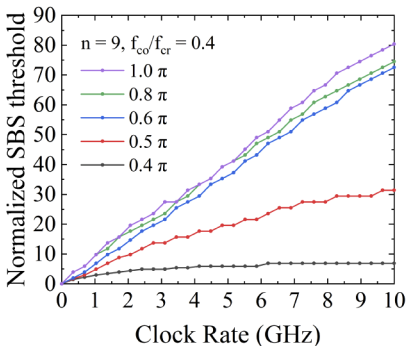

(b) with low-pass filter and RF amplifier for different values of k_σ (or k_{RMS})

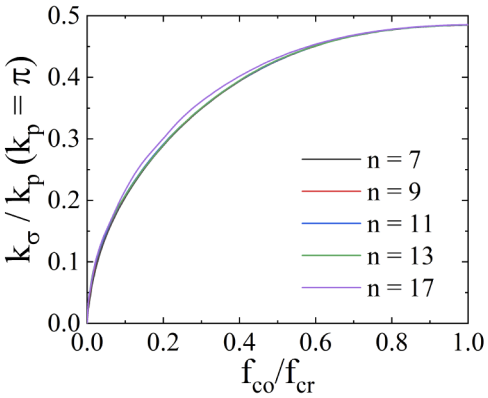

(c) k_σ/k_p vs. f_{co}/f_{cr}, MLS $(-\pi/2, \pi/2)$

Fig. 11. The normalized SBS suppression of MLS9 vs. clock rate for (a) different f_{co}/f_{cr} and (b) different k_σ ($f_{co}/f_{cr} = 0.4$). (c) k_σ/k_p vs. f_{co}/f_{cr} with $f_{cr} = 10$ GHz for different n ($k_p = \pi$).

If SBS is to be suppressed without regard to linewidth, Fig. 12(a) suggests it is best to use a large modulation depth, where suppression is good and the structure is reduced. However, as mentioned, modulation depths k_σ larger than π are difficult to reach because of limitations on the half-wave voltage and the maximum RF input power of commonly used EOPMs. We therefore restrict further investigations to k_σ below π, and use numerical simulations to find the dependence of the normalized SBS threshold on both f_{co}/f_{cr} and k_σ for $n = 3, 5, 7, 9, 11$ with $f_{cr} = 6.5$ GHz in this regime. The results are shown in Fig. 14(a)–14(e). For a large pattern power n, especially $n = 9$, a distinct curve for the local maximum of the normalized SBS threshold appears (see Fig. 14(d)). By comparing Fig. 14(a)–14(e), we find that the global maximum for MLS9 outperforms the other patterns for $k_\sigma < \pi$, and reaches the maximum around $f_{co}/f_{cr} = 0.54$ and $k_\sigma = 0.56\pi$ within the investigated parameter range. The corresponding optical spectrum is shown in Fig. 13(e). Figure 14(a)–14(e) also indicate that a minimum value of f_{co}/f_{cr} of 0.3~0.4 and of k_σ of 0.5π is needed for high SBS suppression. To further distinguish the SBS suppression capability from different patterns, we plot the dependence of the normalized SBS threshold on the modulation depth k_σ with $f_{cr} = 6.5$ GHz and $f_{co}/f_{cr} = 0.4$ in Fig. 14(f). These corresponds to cuts through the Fig. 14(a)–14(e) at $f_{co}/f_{cr} = 0.4$. It is clear from this figure that the $n = 9$ pattern is superior to other patterns for k_σ more than 0.5π. We also calculate the normalized SBS

Optics EXPRESS

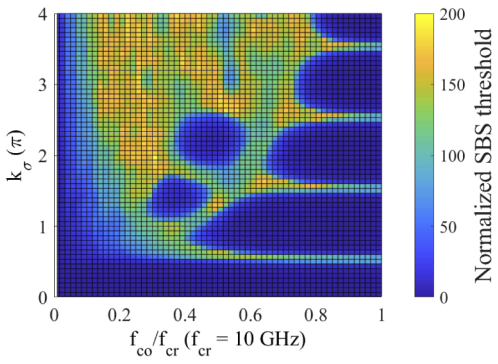

(a) Normalized SBS threshold vs. f_{co}/f_{cr} and k_σ

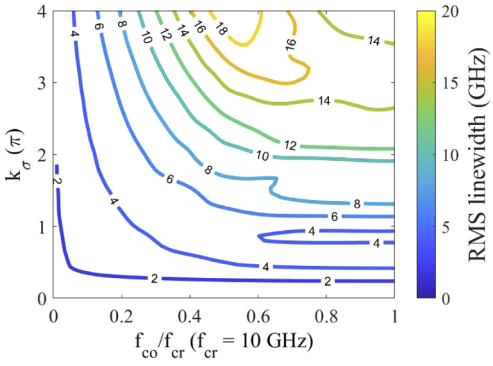

(b) RMS linewidth vs. f_{co}/f_{cr} and k_σ

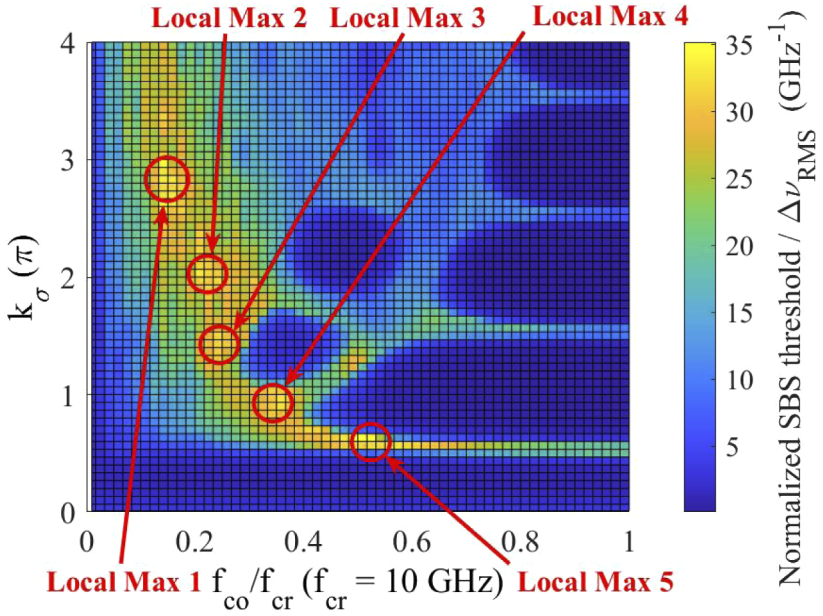

(c) Normalized SBS threshold / RMS linewidth vs. f_{co}/f_{cr} and k_σ

Fig. 12. The normalized SBS suppression vs. f_{co}/f_{cr} and k_σ for MLS9 takes values of -$\pi/2$ or $\pi/2$. (b) The RMS linewidth vs. f_{co}/f_{cr} and k_σ. (c) The ratio of normalized SBS threshold to RMS linewidth vs. f_{co}/f_{cr} and k_σ. Five local maxima are marked in red circle.

Optics EXPRESS

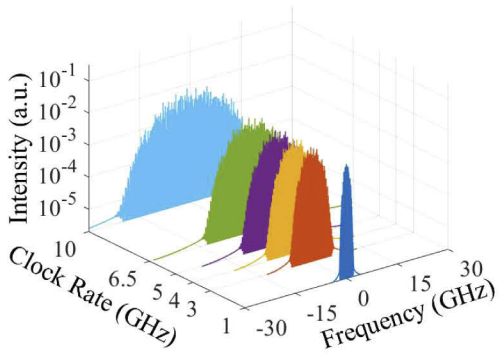

(a) Local maximum 1: $f_{co}/f_{cr} = 0.15$, $k_\sigma = 2.6\pi$

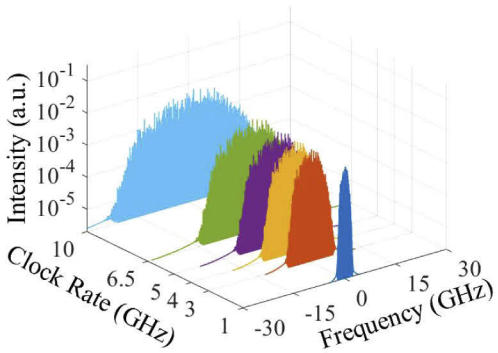

(b) Local maximum 2: $f_{co}/f_{cr} = 0.22$, $k_\sigma = 2\pi$

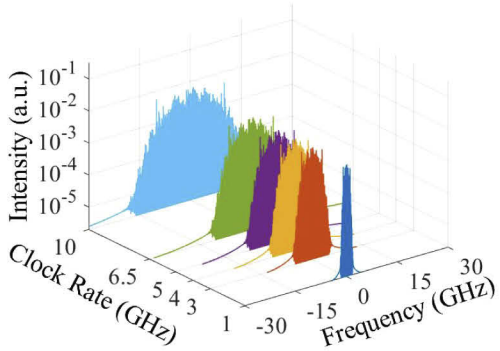

(c) Local maximum 3: $f_{co}/f_{cr} = 0.23$, $k_\sigma = 1.4\pi$

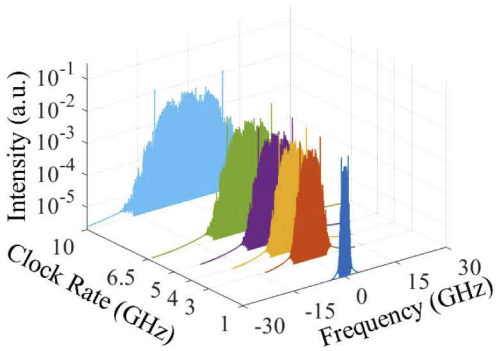

(d) Local maximum 4: $f_{co}/f_{cr} = 0.35$, $k_\sigma = 0.93\pi$

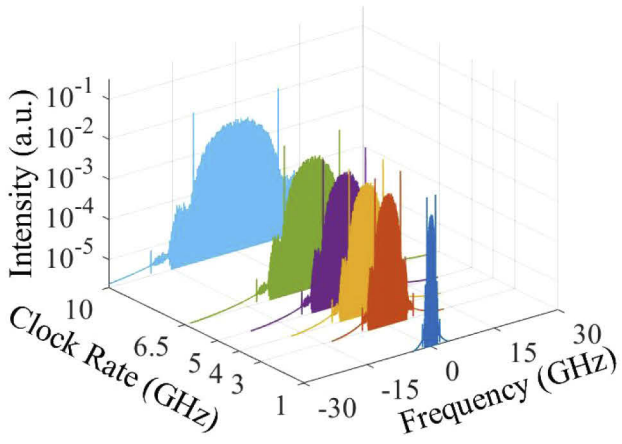

(e) Local maximum 5: $f_{co}/f_{cr} = 0.54$, $k_\sigma = 0.56\pi$

Fig. 13. Power spectra of optical signal as phase modulated by filtered and amplified MLS waveform with f_{co}/f_{cr} and k_σ taking values of (a) $f_{co}/f_{cr} = 0.15$, $k_\sigma = 2.6\pi$ (local maximum 1), (b) $f_{co}/f_{cr} = 0.22$, $k_\sigma = 2\pi$ (local maximum 2), (c) $f_{co}/f_{cr} = 0.23$, $k_\sigma = 1.4\pi$ (local maximum 3), (d) $f_{co}/f_{cr} = 0.35$, $k_\sigma = 0.93\pi$ (local maximum 4), and (d) $f_{co}/f_{cr} = 0.54$, $k_\sigma = 0.56\pi$ (local maximum 5). $f_{cr} = 10$ GHz.

Optics EXPRESS

threshold for MLS9 with clock rate of 1 GHz, 3 GHz, 4 GHz, 5 GHz, 6.5 GHz and 10 GHz, as shown in Fig. 15(a)–15(f). Figure 15(f) is a subset of Fig. 12(a). It is shown that the maximum of the normalized SBS threshold depends on f_{co}/f_{cr} but not the absolute value of f_{cr}.

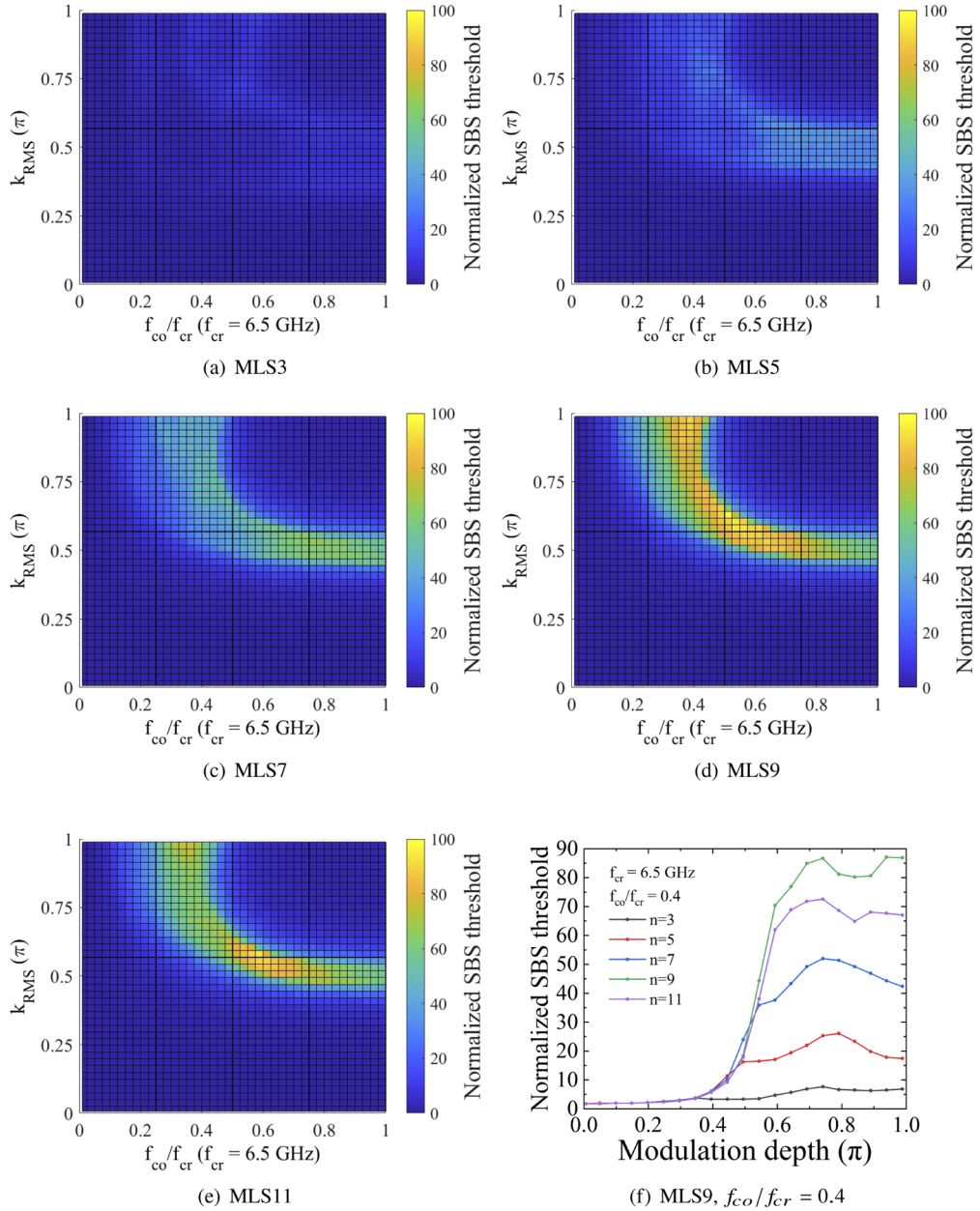

Fig. 14. Normalized SBS threshold vs. f_{co}/f_{cr} and k_σ (or k_{RMS}) for (a) MLS3, (b) MLS5, (c) MLS7, (d) MLS9, and (e) MLS11 with 6.5 GHz clock rate. (f) The normalized SBS threshold vs. k_σ for different patterns ($f_{co}/f_{cr} = 0.4$).

Returning to Fig. 13(e), this contains spectra for the optimized parameters ($f_{co}/f_{cr} = 0.54$ and $k_\sigma = 0.56\pi$) for MLS9 with clock rates of 1 GHz, 3 GHz, 5 GHz, 6.5 GHz, and 10 GHz. For all the clock rates, there are strong components at f_{cr}. We calculate the RMS optical linewidth of

Optics EXPRESS

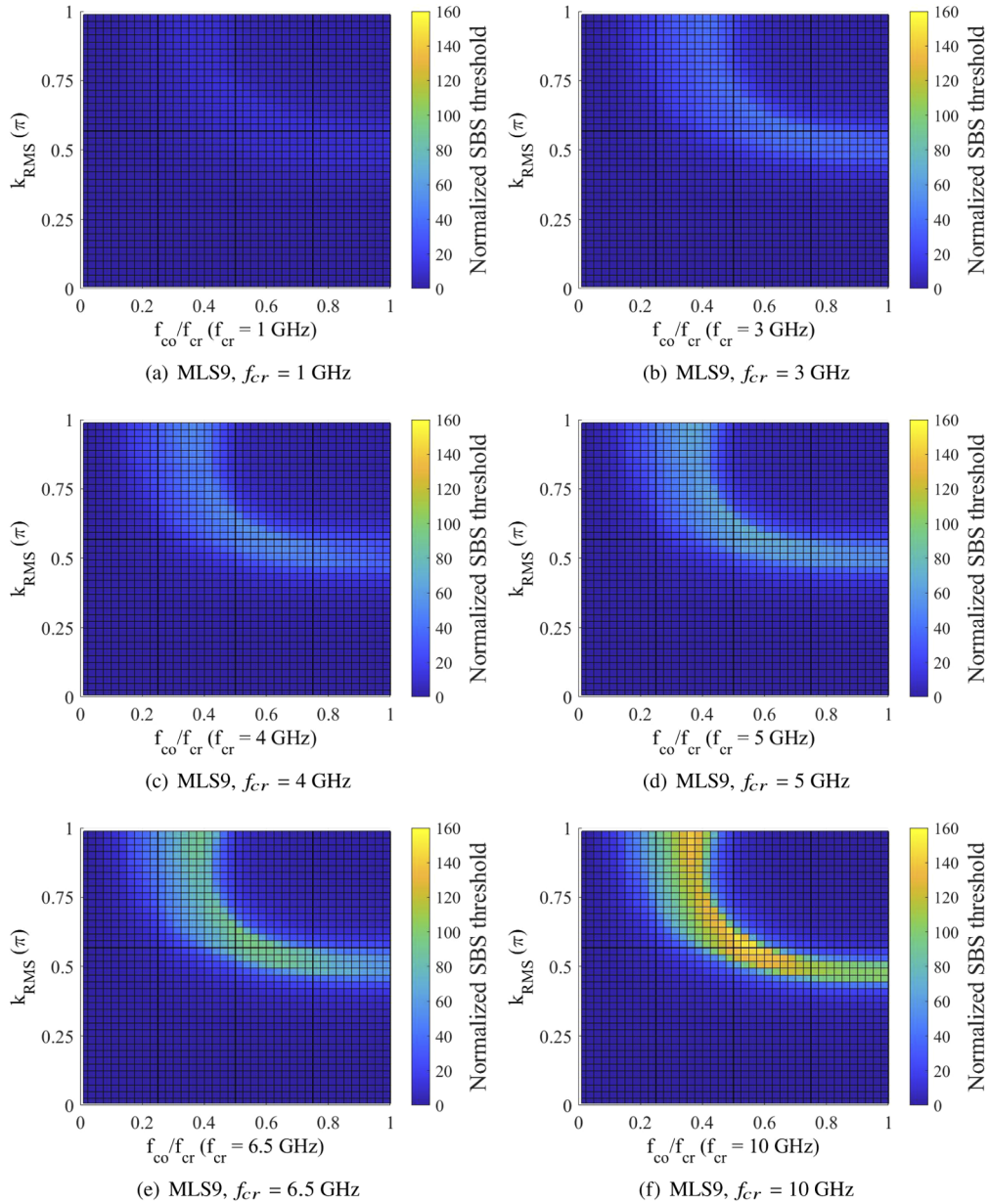

(a) MLS9, f_{cr} = 1 GHz (b) MLS9, f_{cr} = 3 GHz

(c) MLS9, f_{cr} = 4 GHz (d) MLS9, f_{cr} = 5 GHz

(e) MLS9, f_{cr} = 6.5 GHz (f) MLS9, f_{cr} = 10 GHz

Fig. 15. Normalized SBS threshold vs. f_{co}/f_{cr} and k_σ for MLS9 with f_{cr} equal to (a) 1 GHz, (b) 3 GHz, (c) 4 GHz, (d) 5 GHz, (e) 6.5 GHz, and (f) 10 GHz.

Optics EXPRESS

this optimized filtered and amplified MLS phase modulation with $f_{cr} \in (0, 10)$ GHz, as shown in Fig. 16. The normalized SBS threshold for MLS9 with $f_{co}/f_{cr} = 0.54$ and $k_\sigma = 0.56\pi$ for $f_{cr} = 1$ GHz, 3 GHz, 4 GHz, 5 GHz, 6.5 GHz, and 10 GHz (also the global maxima in Fig. 15) is also shown in Fig. 16 (red circles). It is shown that both the RMS linewidth of the optical spectra and the maximum normalized SBS threshold with the optimized parameters increase linearly with f_{cr}, although a roll-off in threshold is expected when the line spacing (which stay below 19.6 MHz in Fig. 16) is sufficiently large, relative to the Brillouin line. The maximum RMS optical linewidth with the parameters considered here is calculated to be within 15 GHz, which indicates that the optimization in this work is suitable for both spectral and coherent beam combining.

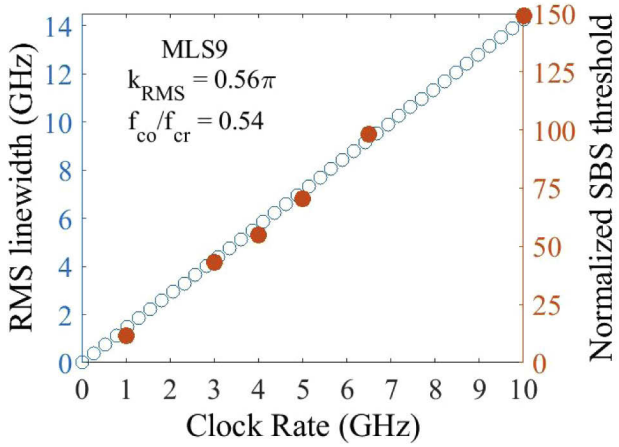

Fig. 16. RMS linewidth (blue circles) of the optical spectra and normalized SBS threshold (red circles) plotted as a function of the clock rate, MLS9, $f_{co}/f_{cr} = 0.54$, $k_\sigma = 0.56\pi$.

The calculations for Fig. 12(a), Fig. 12(c), Fig. 14(a)–14(e) and Fig. 15 are time consuming even for the 61×61 grid that we use, because the SBS threshold is found by numerical iteration with an increasing laser power, incremented in small laser power steps to ensure the accuracy. During the integration, the power increment is adapted to reduce the number of iterations to save computation time: first, we choose a relatively big power increment (20 W). Then the iteration goes quickly through the linear zone of the SBS reflectivity vs. G curve. The nonlinear zone of the reflectivity curve needs a smaller increment to achieve a high accuracy. When the calculated SBS reflectivity exceeds 1% (i.e., when the laser power is above our definition of the threshold), the iteration is repeated from a low power with a new increment which is the previous increment divided by 2. A solution is found when, the SBS reflectivity deviates from the threshold of 1% by less than 1×10^{-6} (relative error $< 10^{-4}$). We use the Parallel Computing Toolbox$^T M$ in Matlab to split the execution of iterations over eight workers in a parallel pool. The execution time for each sub-figure in Fig. 12(a), Fig. 12(c), Fig. 14(a)–14(e) and Fig. 15 is less than 12 hours. Further optimization of the algorithm for threshold searching can improve the computational efficiency.

6. Conclusion

We have investigated SBS suppression in a 7.4-m-long passive fiber through phase-modulation of a single-frequency lightwave with a maximal-length sequence, assumed to be a RF wave. We considered ideal sequences comprising undistorted rectangular bits with π phase difference between symbols, as well as those that were low-pass-filtered and amplified to different levels of phase modulation. The temporal and spectral characteristics of the modulation waveform and the modulated lightwave were investigated analytically with expressions we derived, as

Optics EXPRESS

well as numerically. The SBS threshold power was evaluated through numerical integration of a time-dependent three-wave coupled nonlinear system that describes the SBS dynamics of the phase-modulated lightwave, and subsequent time-averaging. The threshold was quantified relative to the threshold for the unbroadened lightwave (the so-called enhancement factor). For an enhancement factor of around 20, we found that the Brillouin Stokes wave can build up exponentially with a sub-nanosecond time constant in our 7.4-m fiber length. This can then reduce the SBS suppressing capability for MLS waveforms at GHz-level clock rate, insofar as these have uninterrupted single-symbol sub-sequences ("runs") extending over several nanoseconds. The combination of a low-pass filter and a RF amplifier can be used to distort the uninterrupted long sub-sequences and improve the phase distribution and SBS suppression with the MLS waveform. Aiming to accomplish the best SBS mitigation, parameters of the filtered and amplified MLS such as pattern length, modulation depth, and the ratio of filter cutoff frequency to clock rate are optimized numerically. The simulations indicate that for a RMS modulation depth of 0.56π and a ratio of filter cutoff frequency to clock rate of 0.54, the normalized SBS threshold reaches a maximum, and that MLS9 is superior to other investigated patterns (but note that MLS8 and MLS10 were not investigated). Unless the modulation is close to an integer multiple of $\pm\pi/2$, a cutoff frequency larger than around 80% of the clock rate leads to lower SBS suppression in the cases we considered, which we attribute to inadequate suppression of the lightwave's carrier. By contrast, there is no upper limit on the modulation depth, beyond which SBS suppression is no longer effective. Nevertheless, the suppression does not increase monotonically with modulation depth, which necessitates a careful selection of waveform parameters. Similarly, the suppression vs. linewidth characteristics vary significantly, and the suppression can be poor even with large linewidths. Our results provide new insights into SBS and its dynamics, relevant for kilowatt-class fiber systems for spectral and coherent beam combining which need to balance the linewidth and the SBS.

Funding. Youth Innovation Promotion Association of the Chinese Academy of Sciences (2020252); National Key Research and Development Program of China (2018YFB0504500); National Natural Science Foundation of China (61705243, 61735007, 61805261); Special Project for Research and Development in Key areas of Guangdong Province (2018B090904001); Air Force Office of Scientific Research (FA9550-17-1-0007).

Acknowledgments. We would like to thank Dr. Jinghua Tang, School of Engineering, University of Southampton for fruitful discussions.

Disclosures. The authors declare no conflicts of interest.

Data availability. Data underlying the results presented in this paper are available in Ref. [31].

References

1. D. J. Richardson, J. Nilsson, and W. A. Clarkson, "High power fiber lasers: current status and future perspectives," J. Opt. Soc. Am. B **27**(11), B63–B92 (2010).
2. C. Jauregui, J. Limpert, and A. Tünnermann, "High-power fibre lasers," Nat. Photonics **7**(11), 861–867 (2013).
3. G. D. Goodno, S. J. McNaught, J. E. Rothenberg, T. S. McComb, P. A. Thielen, M. G. Wickham, and M. E. Weber, "Active phase and polarization locking of a 1.4 kW fiber amplifier," Opt. Lett. **35**(10), 1542–1544 (2010).
4. S. Kablukov, E. Zlobina, E. Podivilov, and S. Babin, "Output spectrum of Yb-doped fiber lasers," Opt. Lett. **37**(13), 2508–2510 (2012).
5. S. Naderi, I. Dajani, T. Madden, and C. Robin, "Investigations of modal instabilities in fiber amplifiers through detailed numerical simulations," Opt. Express **21**(13), 16111–16129 (2013).
6. M. N. Zervas and C. A. Codemard, "High power fiber lasers: A review," IEEE J. Sel. Top. Quantum Electron. **20**(5), 219–241 (2014).
7. T. Y. Fan, "Laser beam combining for high-power, high-radiance sources," IEEE J. Sel. Top. Quantum Electron. **11**(3), 567–577 (2005).
8. S. J. Augst, J. K. Ranka, T. Fan, and A. Sanchez, "Beam combining of ytterbium fiber amplifiers," J. Opt. Soc. Am. B **24**(8), 1707–1715 (2007).
9. C. Wirth, O. Schmidt, I. Tsybin, T. Schreiber, T. Peschel, F. Brückner, T. Clausnitzer, J. Limpert, R. Eberhardt, A. Tünnermann, M. Gowin, E. ten Have, K. Ludewigt, and M. Jung, "2 kW incoherent beam combining of four narrow-linewidth photonic crystal fiber amplifiers," Opt. Express **17**(3), 1178–1183 (2009).
10. T. H. Loftus, A. Liu, P. R. Hoffman, A. M. Thomas, M. Norsen, R. Royse, and E. Honea, "522 W average power, spectrally beam-combined fiber laser with near-diffraction-limited beam quality," Opt. Lett. **32**(4), 349–351 (2007).

Optics EXPRESS

11. P. Madasamy, D. R. Jander, C. D. Brooks, T. H. Loftus, A. M. Thomas, P. Jones, and E. C. Honea, "Dual-grating spectral beam combination of high-power fiber lasers," IEEE J. Sel. Top. Quantum Electron. **15**(2), 337–343 (2009).
12. C. Wirth, O. Schmidt, I. Tsybin, T. Schreiber, R. Eberhardt, J. Limpert, A. Tünnermann, K. Ludewigt, M. Gowin, E. Ten Have, and M. Jung, "High average power spectral beam combining of four fiber amplifiers to 8.2 kW," Opt. Lett. **36**(16), 3118–3120 (2011).
13. Y. Zheng, Y. Yang, J. Wang, M. Hu, G. Liu, X. Zhao, X. Chen, K. Liu, C. Zhao, B. He, and J. Zhou, "10.8 kW spectral beam combination of eight all-fiber superfluorescent sources and their dispersion compensation," Opt. Express **24**(11), 12063–12071 (2016).
14. B. Anderson, A. Flores, R. Holten, and I. Dajani, "Comparison of phase modulation schemes for coherently combined fiber amplifiers," Opt. Express **23**(21), 27046–27060 (2015).
15. N. A. Naderi, A. Flores, B. M. Anderson, and I. Dajani, "Beam combinable, kilowatt, all-fiber amplifier based on phase-modulated laser gain competition," Opt. Lett. **41**(17), 3964–3967 (2016).
16. A. V. Harish and J. Nilsson, "Optimization of phase modulation formats for suppression of stimulated Brillouin scattering in optical fibers," IEEE J. Sel. Top. Quantum Electron. **24**(3), 1–10 (2018).
17. C. Zeringue, I. Dajani, S. Naderi, G. T. Moore, and C. Robin, "A theoretical study of transient stimulated Brillouin scattering in optical fibers seeded with phase-modulated light," Opt. Express **20**(19), 21196–21213 (2012).
18. A. Flores, C. Robin, A. Lanari, and I. Dajani, "Pseudo-random binary sequence phase modulation for narrow linewidth, kilowatt, monolithic fiber amplifiers," Opt. Express **22**(15), 17735–17744 (2014).
19. M. Howerton and W. Burns, "Depolarized source for high power remote operation of an integrated optical modulator," IEEE Photonics Technol. Lett. **6**(1), 115–117 (1994).
20. A. V. Harish and J. Nilsson, "Optimization of phase modulation with arbitrary waveform generators for optical spectral control and suppression of stimulated Brillouin scattering," Opt. Express **23**(6), 6988–6999 (2015).
21. B. M. Anderson, A. Flores, and I. Dajani, "Filtered pseudo random modulated fiber amplifier with enhanced coherence and nonlinear suppression," Opt. Express **25**(15), 17671–17682 (2017).
22. M. Liu, Y. Yang, H. Shen, J. Zhang, X. Zou, H. Wang, L. Yuan, Y. You, G. Bai, B. He, and J. Zhou, "1.27 kW, 2.2 GHz pseudo-random binary sequence phase modulated fiber amplifier with Brillouin gain-spectrum overlap," Sci. Rep. **10**(1), 629 (2020).
23. E. Lichtman, R. G. Waarts, and A. A. Friesem, "Stimulated Brillouin scattering excited by a modulated pump wave in single-mode fibers," J. Lightwave Technol. **7**(1), 171–174 (1989).
24. M. S. Bowers and N. M. Luzod, "Stimulated Brillouin scattering in optical fibers with end reflections excited by broadband pump waves," Opt. Eng. **58**(10), 1 (2019).
25. R. W. Boyd, K. Rzaewski, and P. Narum, "Noise initiation of stimulated Brillouin scattering," Phys. Rev. A **42**(9), 5514–5521 (1990).
26. V. Kovalev, R. Harrison, and A. Scott, "The build-up of stimulated Brillouin scattering excited by pulsed pump radiation in a long optical fibre," Opt. Commun. **185**(1-3), 185–189 (2000).
27. I. Bar-Joseph, A. Friesem, E. Lichtman, and R. Waarts, "Steady and relaxation oscillations of stimulated Brillouin scattering in single-mode optical fibers," J. Opt. Soc. Am. B **2**(10), 1606–1611 (1985).
28. H.-J. Zepernick and A. Finger, *Pseudo random signal processing: theory and application* (John Wiley & Sons, 2013).
29. W. H. Press, H. William, S. A. Teukolsky, W. T. Vetterling, A. Saul, and B. P. Flannery, *Numerical recipes 3rd edition: The art of scientific computing* (Cambridge university press, 2007).
30. F. Gustafsson, "Determining the initial states in forward-backward filtering," IEEE Trans. Signal Process **44**(4), 988–992 (1996).
31. Y. Yang, B. Li, M. Liu, X. Huang, Y. Feng, D. Cheng, B. He, J. Zhou, and J. Nilsson, "Provide title," University of Southampton repository, 2021, https://doi.org/10.5258/SOTON/D1795. Q2